Biofabrication

PAPER

Vascular smooth muscle cells can be circumferentially aligned inside a channel using tunable gelatin microribbons

To cite this article: Yusuf Mastoor *et al* 2025 *Biofabrication* **17** 015011

IOP Publishing Biofabrication 17 (2025) 015011 https://doi.org/10.1088/1758-5090/ad88a7

Biofabrication

PAPER

Vascular smooth muscle cells can be circumferentially aligned inside a channel using tunable gelatin microribbons

Yusuf Mastoor[1], Mahsa Karimi[3], Michael Sun[1], Fereshteh Ahadi[3], Pattie Mathieu[1], Mingyue Fan[2], Lin Han[2], Li-Hsin Han[3] and Alisa Morss Clyne[1,*]

[1] Fischell Department of Bioengineering, University of Maryland, 8278 Paint Branch Drive, College Park, MD 20742, United States of America
[2] School of Biomedical Engineering, Science and Health Systems, 3141 Chestnut St, Philadelphia, PA 19104, United States of America
[3] Department of Mechanical Engineering and Mechanics, Drexel University, 3141 Chestnut St, Philadelphia, PA 19104, United States of America
[*] Author to whom any correspondence should be addressed.

E-mail: aclyne@umd.edu

RECEIVED
19 April 2024

REVISED
4 September 2024

ACCEPTED FOR PUBLICATION
18 October 2024

PUBLISHED
30 October 2024

Keywords: vascular smooth muscle cells, microribbons, hydrogel, cell alignment, artery-on-a-chip

Supplementary material for this article is available online

Abstract

The gold standard to measure arterial health is vasodilation in response to nitric oxide. Vasodilation is generally measured via pressure myography of arteries isolated from animal models. However, animal arteries can be difficult to obtain and may have limited relevance to human physiology. It is, therefore, critical to engineer human cell-based arterial models capable of contraction. Vascular smooth muscle cells (SMCs) must be circumferentially aligned around the vessel lumen to contract the vessel, which is challenging to achieve in a soft blood vessel model. In this study, we used gelatin microribbons to circumferentially align SMCs inside a hydrogel channel. To accomplish this, we created tunable gelatin microribbons of varying stiffnesses and thicknesses and assessed how SMCs aligned along them. We then wrapped soft, thick microribbons around a needle and encapsulated them in a gelatin methacryloyl hydrogel, forming a microribbon-lined channel. Finally, we seeded SMCs inside the channel and showed that they adhered best to fibronectin and circumferentially aligned in response to the microribbons. Together, these data show that tunable gelatin microribbons can be used to circumferentially align SMCs inside a channel. This technique can be used to create a human artery-on-a-chip to assess vasodilation via pressure myography, as well as to align other cell types for 3D *in vitro* models.

1. Introduction

Cardiovascular disease (CVD) is the leading cause of death globally [1]. For many patients, CVD manifests as atherosclerosis, in which fibrous and fatty material accumulates in the blood vessel wall. Atherosclerosis can eventually lead to myocardial infarction or stroke [2]. Initial endothelial dysfunction allows lipids to permeate into the vascular wall, forming the atherosclerotic plaque. Endothelial dysfunction is characterized by reduced nitric oxide (NO) formation and bioavailability, which leads to impaired endothelial-dependent vasodilation [3, 4]. In healthy blood vessels, NO is synthesized by endothelial cells to regulate vascular tone by signaling the underlying vascular smooth muscle cells (SMCs) to relax [5].

Since NO is difficult to measure *in vitro*, endothelial NO is often measured as vasodilation of ex vivo mouse vessels via pressure myography. In this procedure, an isolated vessel is cannulated and intraluminally pressurized to study the effects of drugs, pressure, and flow on vascular diameter [6, 7]. Changes in vascular diameter can be attributed to SMC health and function [8]. However, pressure myography is challenging to implement in many laboratories. The vessels used are from mice, which may have limited applicability to humans, and the impact of perivascular tissues on blood vessels is difficult to measure [9]. Current *in vitro* vessel-on-a-chip models are generally tubular monolayers of axially aligned endothelial cells (ECs) in microchannels, which can be used to test transport across

endothelial barriers [10, 11] but do not account for SMC function. More advanced tissue-engineered arteries capable of contraction have been developed; however, these require complex culture conditions for long periods of time, making them challenging to implement [12]. It is, therefore, critical to develop physiologically relevant human blood vessel models capable of recapitulating SMC vasoconstriction and vasodilation *in vitro*.

Circumferential alignment of SMCs inside a channel is essential to achieve a contractile artery-on-a-chip [13, 14]. While SMCs will align in response to applied cyclic stretch, this process takes on the order of days [15]. SMCs align more quickly when seeded on topographically patterned surfaces. A variety of methods have been developed to align SMCs on flat, 2D substrates, including micropatterning lines of adhesive polystyrene [16], fibronectin [17], or collagen onto tissue culture plastic dishes [18]. Another method involves directly microfabricating ridges through soft photolithography [19] or using the ridges inherent to the fused deposition modeling 3D printing process [20]. Once aligned on these patterned substrates, SMCs increased expression of smooth muscle myosin heavy chain, a marker for contractile cells, and decreased cell proliferation and migration [19, 21, 22]. While these methods work well to align SMCs, they are often complex and work on a limited number of 2D substrates.

SMC circumferential alignment in a cylindrical channel has been achieved by inducing UV-microwrinkles on PDMS [23], 3D bioprinting GelMA springs [24], and using alginate fibers [21]. While SMCs can be circumferentially aligned using these methods, they require high substrate stiffness and large channel diameters, which are not ideal for recapitulating an artery *in vitro*. With advances in tissue engineering, ribbon scaffolds made from a variety of materials, including alginate [21], dextran [25], and polycaprolactone [26, 27], have been used to align SMCs in 3D. However, these synthetic materials often have stiffnesses that are orders of magnitude greater than the blood vessel wall. When cultured on substrates with high stiffness, SMCs are less contractile [27].

Recently, gelatin microribbons were developed as an alternative method to align cells, including SMCs [28, 29]. When bladder-derived SMCs were seeded on a flat monolayer of aligned gelatin microribbons, the cells increased expression of myosin heavy chain, a protein critical to SMC contractile phenotype [30]. Notably, the gelatin microribbons can induce and maintain cell alignment when added to a hydrogel for 3D cell culture, whereas achieving cell alignment in 3D hydrogels is challenging due to constraints imposed by the hydrogel's nanoporous network [31]. Gelatin microribbon physical properties, including stiffness and diameter, can be used to modulate 3D cell shape, cytoskeleton morphology, and mechanotransduction [29]. In one study, gelatin microribbons maintained mesenchymal stem cell (MSC) alignment within a hydrogel for 21 d, which accelerated cartilage formation and stiffness [28, 32].

In this study, we determined how gelatin microribbons could circumferentially align SMCs within a cylindrical channel to quickly recapitulate *in vivo* vascular architecture *in vitro*. We tested SMC viability and alignment on thin and thick, soft and stiff gelatin microribbons. We then developed a method to wrap microribbons around a needle, encapsulate the microribbons in a hydrogel, and seed SMC on the circumferentially aligned microribbons. This method can be used to circumferentially align SMCs inside a channel, which is essential to creating a contractile artery-on-a-chip in the future.

2. Materials and methods

2.1. Microribbon synthesis and preparation

Gelatin fibers were synthesized as previously described [29]. Briefly, Type A porcine gelatin (Sigma Aldrich G2500) was dissolved in deionized water in a 1:1 weight:volume (w:v) ratio. Gelatin was then injected into a hollow polycaprolactone (PCL, Thermomorph, 4336898380) rod (inner diameter: 3 mm, outer diameter: 15 mm) and heat-sealed using melted PCL. The PCL rod was heated to 80 °C and folded, and the two ends of the rod were fused together. The newly formed PCL ring was then repeatedly stretched, twisted, and folded at 80 °C, with the ends fused together after each fold. To form thin microribbons, the PCL was folded 18 times. For thick microribbons, the PCL was folded 13 times. Gelatin microribbons were extracted by dissolving the PCL cladding around the gelatin using a 9:1 volume:volume (v:v) mixture of acetone (Fisher Scientific, A949) and chloroform (Fisher Scientific, A412P). To enhance microribbon durability and reduce breakage during wrapping, microribbons were treated with 0.53% succinic acid and 0.2% glutaraldehyde. To modulate stiffness, microribbons were treated with varying percentages of methacrylate anhydride (MAA; Sigma Aldrich, 276685) and acetic anhydride (Sigma–Aldrich, 242845) in methanol for 24 h at 40 °C. Stiff microribbons were treated with 0.4% v:v MAA in methanol, while soft microribbons were treated with 0.08% v:v MAA and 0.3% v:v acetic anhydride in methanol. Microribbons were then thoroughly washed, dialyzed, lyophilized, and stored at −20 °C until use. Gelatin microribbon synthesis details are summarized in table 1.

For fibronectin coating, dry microribbons were rehydrated in 5 μg ml^{-1} fibronectin solution (Sigma-Aldrich, F0895). After five minutes, the excess fibronectin solution was removed, and the sample was air-dried for 45 min at room temperature prior to use.

Table 1. Microribbon type based on fold number and chemical treatment.

Microribbon type	Fold number	Methacrylate anhydride (v:v)	Acetic anhydride (v:v)	Glutaraldehyde (v:v)	Succinic acid (v:v)
Thin, Soft	18 folds	0.08%	0.3%	0.2%	0.16%
Thin, Stiff	18 folds	0.4%	0%	0.2%	0.16%
Thick, Soft	13 folds	0.08%	0.3%	0.2%	0.16%
Thick, Stiff	13 folds	0.4%	0%	0.2%	0.16%

2.2. GelMA synthesis and microribbon encapsulation

Gelatin methacryloyl (GelMA) was synthesized by dissolving 10% w/v Type A porcine gelatin in phosphate buffered saline (PBS) at 50 °C. 7.6% v:v MAA was added dropwise to the gelatin solution over 90 min. The solution was centrifuged at 600 g for 5 min to pellet unreacted MAA. The supernatant was then diluted with an equal amount of PBS and dialyzed over two days using a dialysis cassette (Thermo Scientific, 66830) submerged in deionized water at 48 °C. After dialysis, the solution pH was adjusted to 7–7.4 using 1 M NaOH. The solution was then lyophilized for five days and stored at room temperature.

To create the GelMA precursor solution, lyophilized GelMA was UV sterilized at 254 nm in a UVP Crosslinker (Analytik Jena, CX-2000) for 30 min and then dissolved in PBS (10% w:v) at 50 °C with 0.05% w/v photoinitiator (lithium phenyl-2,4,6-trimethylbenzoylphosphinate; LAP, Sigma, 900889).

Microribbons were added to 10% w/v GelMA precursor solution to embed microribbons in GelMA. The mixture of microribbons and GelMA precursor was UV crosslinked at 254 nm for up to two minutes.

2.3. GelMA modulus via unconfined compression testing

GelMA bulk modulus was determined via unconfined compression tests using a MARK-10 compression tester with a Series 5 digital force gauge (9024100000) and a 10 N load cell. GelMA with 0.05% (v/v) LAP was poured into a silicone mold (6 mm diameter, 3 mm thickness), positioned between two glass slides, and immediately UV crosslinked. The GelMA disc diameter and thickness were measured using digital calipers and then placed in PBS for testing. A 2 mN preload was applied to each disk to ensure complete contact between the GelMA surface and the upper plate. The upper plate was then lowered at 10 mm min^{-1} until a maximum strain of 20% was achieved. Load and displacement data were recorded at 10 Hz for eight samples. A GelMA modulus of 24.63 ± 4.09 kPa was calculated using the stress–strain curve in the 10%–20% strain range.

2.4. Microribbon modulus via AFM-nanoindentation

The effective modulus, E_{ind}, of microribbons was determined via atomic force microscopy (AFM)-based nanoindentation, following our established procedure [33]. In brief, guided by the optical microscope of the AFM, nanoindentantion was performed on microribbons using microspherical colloidal tips ($R \approx 5$ μm, nominal $k \approx 0.03$ N m^{-1}, NanoAndMore, Arrow-TL1Au) and a Dimension Icon AFM (Bruker Nano) in 1× PBS. The indentation was carried out at a constant z-piezo displacement rate of 10 μm s^{-1} up to a maximum indentation force of 40 nN. For each type of sample, a minimum of 15 different microribbons were tested to account for heterogeneity. The effective indentation modulus, E_{ind}, was calculated by fitting the entire portion of each force versus distance (F-D) loading curve to the finite thickness-corrected Hertz model [34], assuming microribbon thickness of ∼10 μm and a Poisson's ratio of 0.49 for highly swollen hydrogels [35].

2.5. Human coronary artery smooth muscle cell culture

Human coronary artery smooth muscle cells (SMC, Lonza, CC- 2583) were maintained in Smooth muscle Growth Medium (SmGM-2, Lonza, CC-3182) supplemented with 10% fetal bovine serum (FBS, HyClone, SH30071.03), 1% penicillin-streptomycin (Gibco, 15140122), and 1% l-glutamine (Gibco, 25030-081). Cells were cultured in a humidified incubator at 37 °C, 5% CO_2 and used between passage 4 and 8. Under these conditions, the SMCs are primarily in a proliferative phenotype. To seed or encapsulate cells, trypsin-EDTA (Gibco, 25200056) was used to chemically detach the cells from the culture dish. Cells were pelleted at 600 g, resuspended in SmGM-2, and then counted using a Countess automated cell counter (Thermo Fisher Scientific, AMQAX1000).

To seed SMCs on microribbons, uncoated and fibronectin-coated microribbons were weighed and rehydrated in SmGM-2. 10^5 SMCs were added per 0.1 g microribbons. Samples were then rocked on an Enduro MiniMix Nutating Mixer (LabNet, S0600) for two hours to spread cells throughout the microribbons. After rocking, microribbons were cultured in static conditions for 48 h prior to imaging.

2.6. Live cell imaging and SMC alignment quantification

SMC viability on microribbons and in GelMA was assessed using a Live/Dead assay (Thermo Scientific, L3224). Cell culture media was aspirated from the

microribbons, and 2 μM calcein-AM and 4 μM ethidium homodimer-1 in PBS were added to cover the microribbons. Samples were incubated for 30 min and then imaged using a Nikon Eclipse Ti2-E confocal laser scanning microscope at 10x magnification with 2.5 μm step sizes. To quantify SMC viability, the maximum intensity projections of the live and dead channels were imported into MATLAB. An intensity threshold, selected to isolate individual cells from the microribbons in the images and to minimize the detection of other particles, was manually applied to each image. The *Fill Holes* command was used to minimize empty cell space, and the *Watershed* operation was then used to separate adjacent cells. The number of particles was counted for both live and dead cell images, and the percentage of live cells compared to total cells was determined. Live/dead assay results were verified using an MTT assay.

Calcein images were also used to quantify cell alignment because live cells could be labeled and imaged, which avoided fixation artifacts and ensured that we were only measuring the alignment of viable cells. Calcein-AM enters the cytoplasm of live cells, where nonspecific esterases cleave the acetoxymethyl ester group to enable free calcein fluorescence in the entire cytoplasm. We verified that cell body alignment via calcein labeling was equally effective as actin measurements (supplemental figure 1). SMC alignment was quantified using MatFiber software as previously described [20, 36]. Briefly, the maximum intensity projection of the calcein channel z stack was adjusted for brightness and contrast and exported as a grayscale image into MATLAB (MathWorks, 2022b). A rectangular region of interest was drawn to isolate an individual microribbon, and the microribbon major axis was determined. This region of the image was then separated into 40 $\times$ 40 pixel square subregions. MatFiber generated a vector for each subregion based on an intensity gradient detection algorithm. The vector angle for each subregion was then normalized to the microribbon major axis angle to determine cell alignment to the microribbon. Alignment was compared among groups by calculating the average of the angle absolute values.

2.7. Microribbon-lined channel

To line the interior surface of a GelMA channel with microribbons, dry microribbons were rehydrated in SmGM-2 for 24 h. Microribbons were then wrapped around a 25 G needle. During the wrapping process, SmGM-2 supplemented with 0.05% LAP was added to the microribbons to keep them hydrated. A 3D-printed device with a 10 $\times$ 24 $\times$ 2 mm central chamber was adhered to a glass coverslip (figure 1(A)). The needle wrapped with microribbons was then placed into the 3D-printed device, and 10% w:v GelMA was added to the chamber to cover the needle completely (figures 1(B)–(D)). A second glass coverslip was adhered to the top of the 3D-printed device with excess GelMA. The device was UV crosslinked at 254 nm for 5 min on both sides. The needle was then removed, exposing the microribbon-lined channel. 10^6 SMCs in 200 μl of SmGM-2 were added to the channel, and the entire device was inverted after 30 min to ensure cell seeding on both sides of the channel. SMCs were cultured on microribbons in the channel for 24 h at 37 °C, 5% CO_2, labeled for live and dead cells, and imaged as previously described.

2.8. Statistical analysis

All statistical analyses were performed with GraphPad Prism software (Version 9.5.1). Data are expressed as mean $\pm$ standard deviation. For comparisons between two groups, a Mann–Whitney test was used to analyze data. For comparisons among multiple groups, a Kruskal–Wallis test with Tukey–Kramer multiple comparisons was used to analyze data.

3. Results

3.1. Gelatin microribbons with varying stiffness and thicknesses

We first synthesized microribbons of different thicknesses and stiffness to determine which microribbons would best enable SMCs to align, as it was previously shown that gelatin microribbon size and stiffness can alter cell properties and function [29]. Thick microribbons ranged from 8.89 to 79.79 μm wide (average: 33.85 μm wide), while thin microribbons ranged from 6.68 to 19.55 μm wide (average: 10.60 μm wide) (figures 2(A) and (B)). Thin microribbons were more than three times smaller than thick microribbons ($p < 0.0001$; figure 2(B)). Soft microribbons had an average elastic modulus of 6.59 kPa, as measured by AFM, which is similar to the elastic modulus of healthy vascular tissue ($\sim$10 kPa) [37]. In contrast, stiff microribbons had an average elastic modulus of 35.08 kPa (figure 2(C)). These data show that microribbons of varying thickness and stiffness can be created using our technique.

3.2. SMCs aligned along individual microribbons

We then seeded SMCs on thin, thick, soft, and stiff microribbons and assessed their viability and alignment. SMCs attached to and lined all microribbons, regardless of microribbon size or stiffness (figure 3(A)). Similarly, SMCs retained their viability on all microribbons, with an average viability greater than 80%. SMC viability on the microribbons was similar to SMC viability on tissue culture polystyrene (TCPS; supplemental figure 1). While SMC viability was similar on soft microribbons regardless of their thickness, SMCs on thin, stiff microribbons (67.21%) had significantly lower viability ($p = 0.036$) as compared to SMCs on thick, soft microribbons (87.24%). When comparing SMCs on thin, stiff microribbons to SMCs on thick, stiff microribbons,

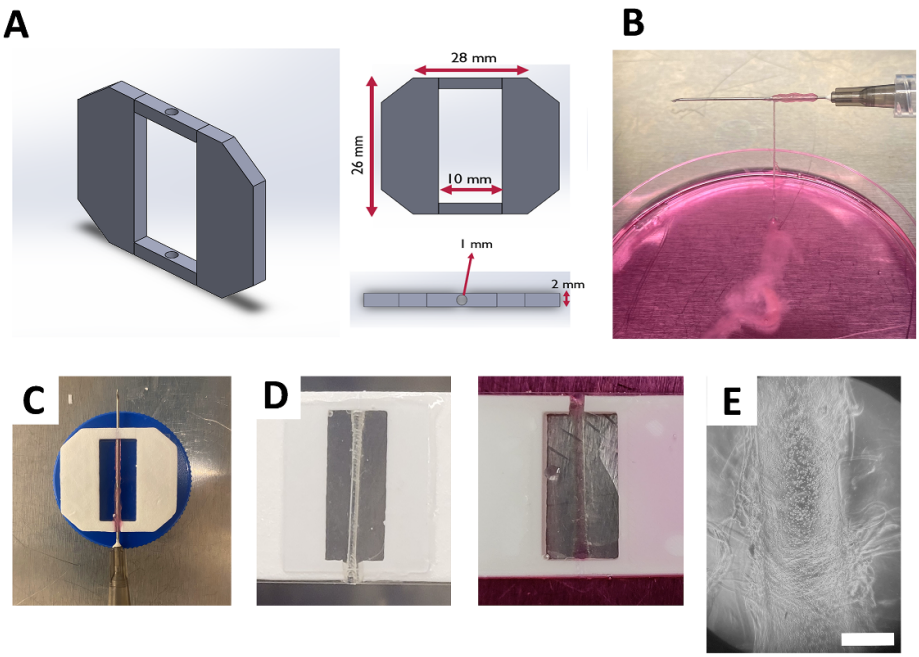

Figure 1. Microribbon-lined channel preparation schematic. (A) 3D printed mold to hold wrapped microribbons and hydrogel during GelMA encapsulation. (B) Representative image of microribbons being wrapped around a needle and (C) placed in the 3D printed mold. (D) Representative image of microribbon channel after GelMA crosslinking and needle removal with media perfused through. (E) Representative phase contrast image of microribbon channel. Scale bar = 500 μm.

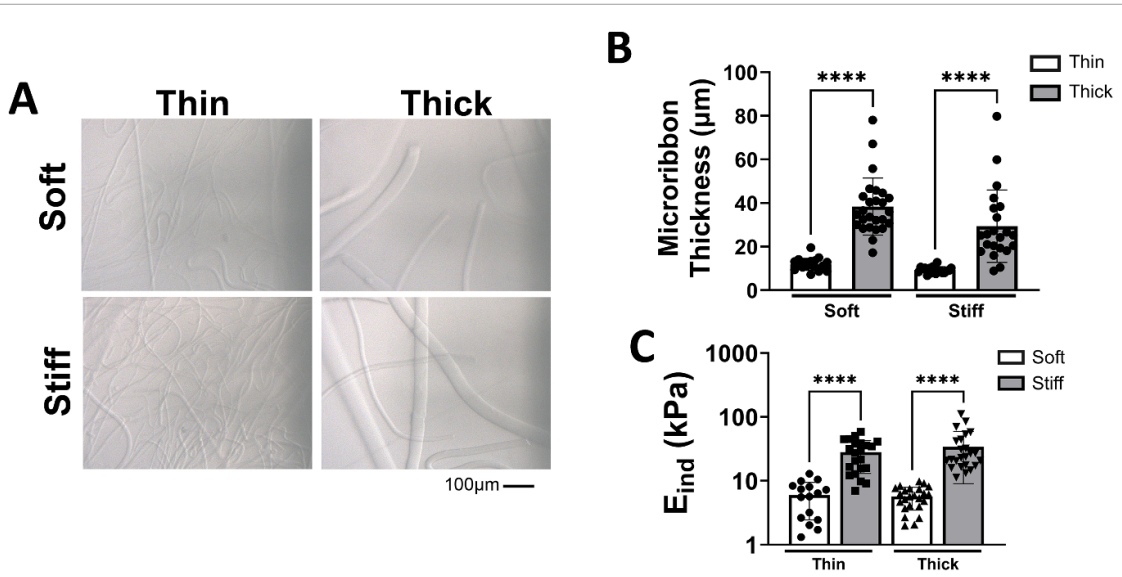

Figure 2. Microribbons were created of varying thicknesses and stiffnesses. (A) Representative phase contrast images of microribbons. (B) Average microribbon thickness. (C) Average effective modulus, E_{ind}, of microribbons. Each sample is an individual microribbon. Statistical significance for (B), (C) determined using a Kruskal–Wallis test followed by Tukey–Kramer multiple comparisons. **** $p < 0.0001$.

there was a trend ($p = 0.058$) for increased SMC viability on thick, stiff microribbons (figure 3(B)). SMCs also spread more on thick microribbons than thin microribbons, indicating more effective cell adhesion, as shown by higher cell area on the thick microribbons than thin microribbons. This was statistically significantly higher for the stiff, thick microribbons as compared to soft and stiff, thin microribbons (figure 3(C)). Taken together, these data show that SMCs had the highest viability and spreading on thick microribbons.

Next, we quantified the alignment of SMCs lining individual microribbons. Thin microribbons were too tightly packed to assess SMC alignment to an individual microribbon. However, SMCs on thick microribbons could be clearly visualized and analyzed for alignment with the microribbon. When individual microribbon sections were isolated, and

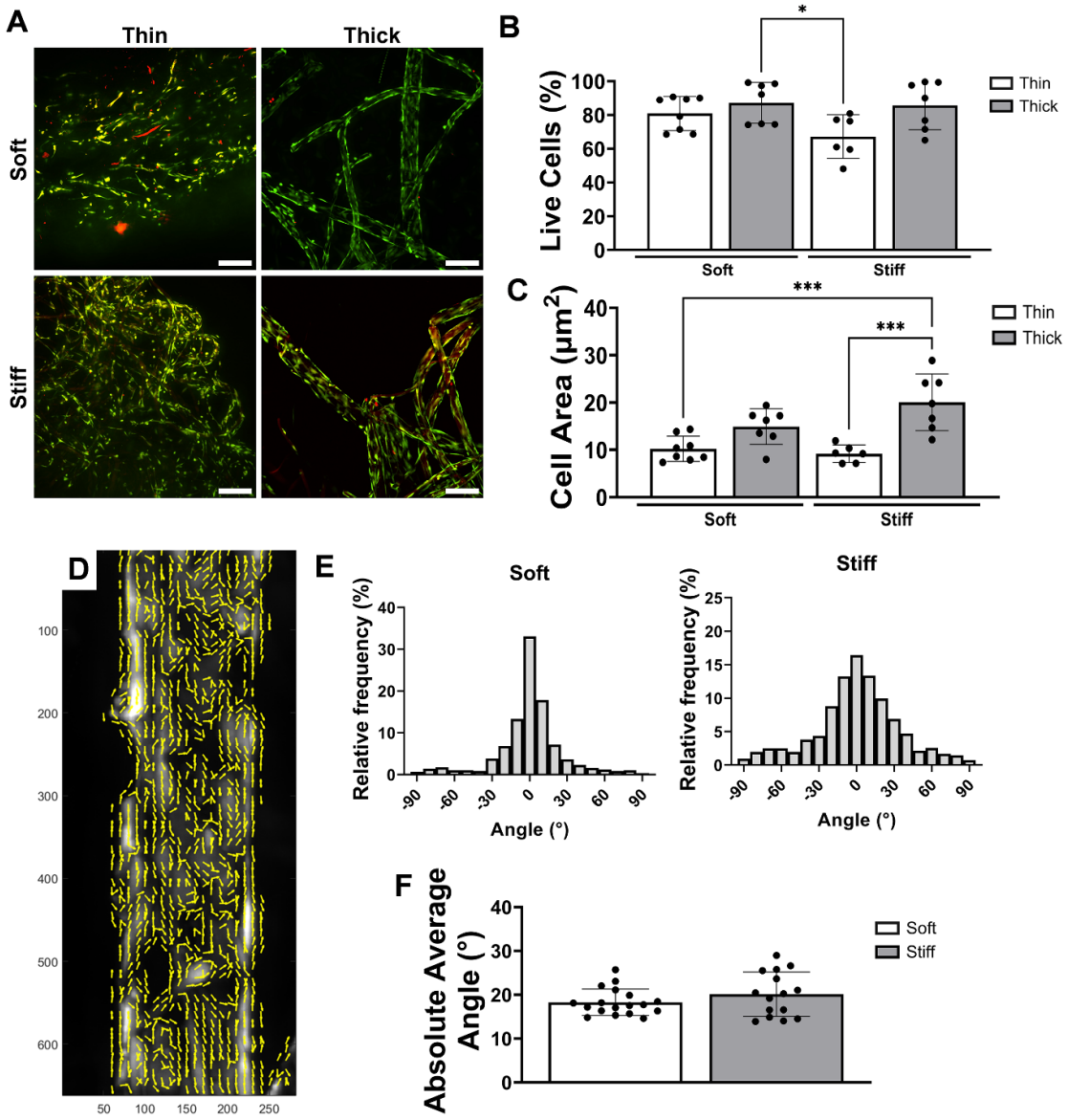

Figure 3. SMCs adhered to and aligned on thick microribbons. (A) Representative confocal microscopy images of SMCs on soft and stiff microribbons of varying thicknesses. Cells were labeled with calcein (green) indicating live cells and ethidium homodimer-1 (red) indicating dead cells. Scale bar = 200 μm. Quantification of the (B) percentage of live cells and (C) cell area. $n = 6$–8 samples. (D) Representative vector alignment of calcein-labeled SMCs on a soft, thick microribbon. (E) Representative alignment angle distributions for thick microribbons. (F) Absolute angles (0-90°) for cells on thick microribbons. $n = 15$–18 individual microribbons from four samples per group. Statistical significance for (B), (C) determined using a Kruskal–Wallis test and for (F) via a Mann–Whitney test. * $p < 0.05$, *** $p < 0.001$.

cell alignment was quantified (figure 3(D)), SMC on thick microribbons of both stiffnesses aligned with the microribbon on which they adhered (figure 3(E)). Regardless of stiffness, cells on thick microribbons had average absolute angles less than 25° (0° represents complete alignment with the microribbon; figure 3(F)). After quantifying SMC alignment to individual microribbons, we chose to use soft, thick microribbons to form the microribbon-lined channel to ensure cells aligned well along each individual microribbon and to keep the channel stiffness similar to that of the vascular wall.

3.3. SMCs circumferentially aligned inside a microribbon-lined channel

We then determined how best to seed SMCs on the microribbons for channel fabrication. When we seeded the cells on microribbons that remained undisturbed, SMCs adhered to (figure 4(A)) and aligned well to the microribbons with an average absolute angle of 21.65° (figure 4(F)). However, when we wrapped the cell-laden microribbons around a 25 G needle, as would be needed for channel formation, cell adhesion (figure 4(B)), viability (figure 4(D)), and alignment (figure 4(F)) were

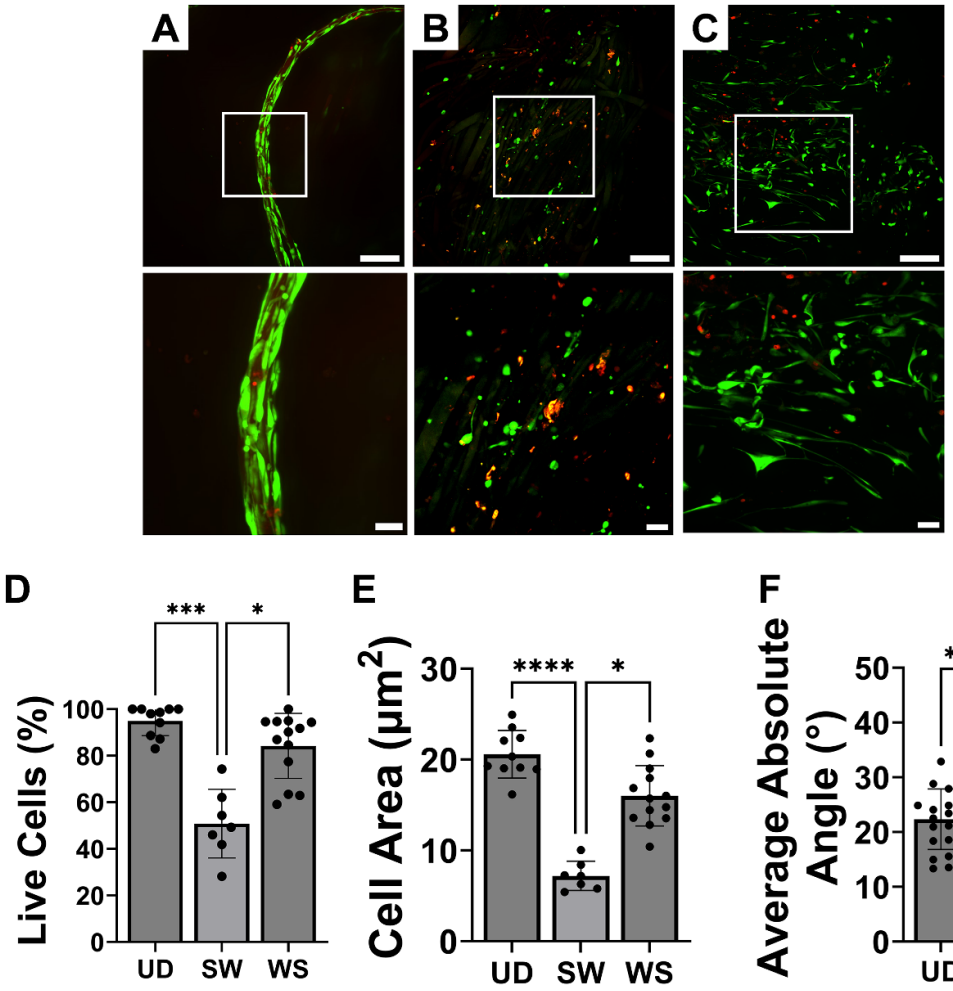

Figure 4. SMC adherence and spreading were higher when cells were seeded after wrapping the microribbons around the needle. Representative confocal microscopy images of SMCs on (A) undisturbed microribbons (UD), (B) microribbons wrapped after cell seeding (SW), (C) microribbons wrapped prior to cell seeding (WS). Scale bar = 200 μm, scale bar for zoomed images = 50 μm. Cells were labeled with calcein (green), indicating live cells, and ethidium homodimer-1 (red), indicating dead cells. Quantification of the (D) percentage of live cells (n = 7–13 samples), (E) cell area (n = 7–13 samples), (F) absolute angle (n = 16–60 individual microribbons from 7–13 samples per group). Statistical significance for (D)–(G) determined using a Kruskal–Wallis test. * $p < 0.05$, *** $p < 0.001$, **** $p < 0.0001$.

severely compromised. When we instead wrapped the microribbons around the needle and then seeded cells on the wrapped microribbons, cells on the wrapped microribbons exhibited similar viability (84%, $p = 0.2886$), spreading (16 μm^2, $p = 0.0655$), and alignment (24°, $p = 0.7037$) as cells on undisturbed microribbons (figures 4(D)–(G)). SMCs seeded on microribbons after wrapping had significantly greater viability ($p = 0.0147$), cell area ($p = 0.0184$), and alignment ($p < 0.0001$) compared to SMCs seeded on microribbons before wrapping (figures 4(D)–(G)). As seeding SMCs on wrapped microribbons increased viability, spreading, and alignment, we chose to seed SMCs on pre-wrapped microribbons to form the final SMC-lined channel.

Since the final microribbon-lined channel would need to be encapsulated in GelMA, we investigated how encapsulating the pre-wrapped, cell seeded microribbons in GelMA would impact cell adhesion to the microribbons. Although SMCs were 90% viable and aligned well (average absolute angle of 28°) on the microribbons immediately after GelMA encapsulation, after 24 h, SMC viability and spread area decreased, suggesting that the cells were detaching from the microribbons (representative images in figure 5(A), quantification in figures 5(B) and (D)). To enhance cell adhesion to the microribbons after GelMA encapsulation, we fibronectin-coated microribbons prior to cell seeding. Fibronectin-coated microribbons had higher SMC viability (84%, $p = 0.0319$) and SMC alignment with the microribbons (24°, $p = 0.0147$) 24 h after encapsulation, as compared to microribbons encapsulated in GelMA for 24 h without fibronectin coating (figures 5(B) and (D)). Fibronectin-coated microribbons also had a lower ($p = 0.004$) average absolute angle immediately after GelMA encapsulation (22°), as compared to SMCs on microribbons without fibronectin coating (28°; figure 5(D)). However, fibronectin coating had no significant effect on SMC

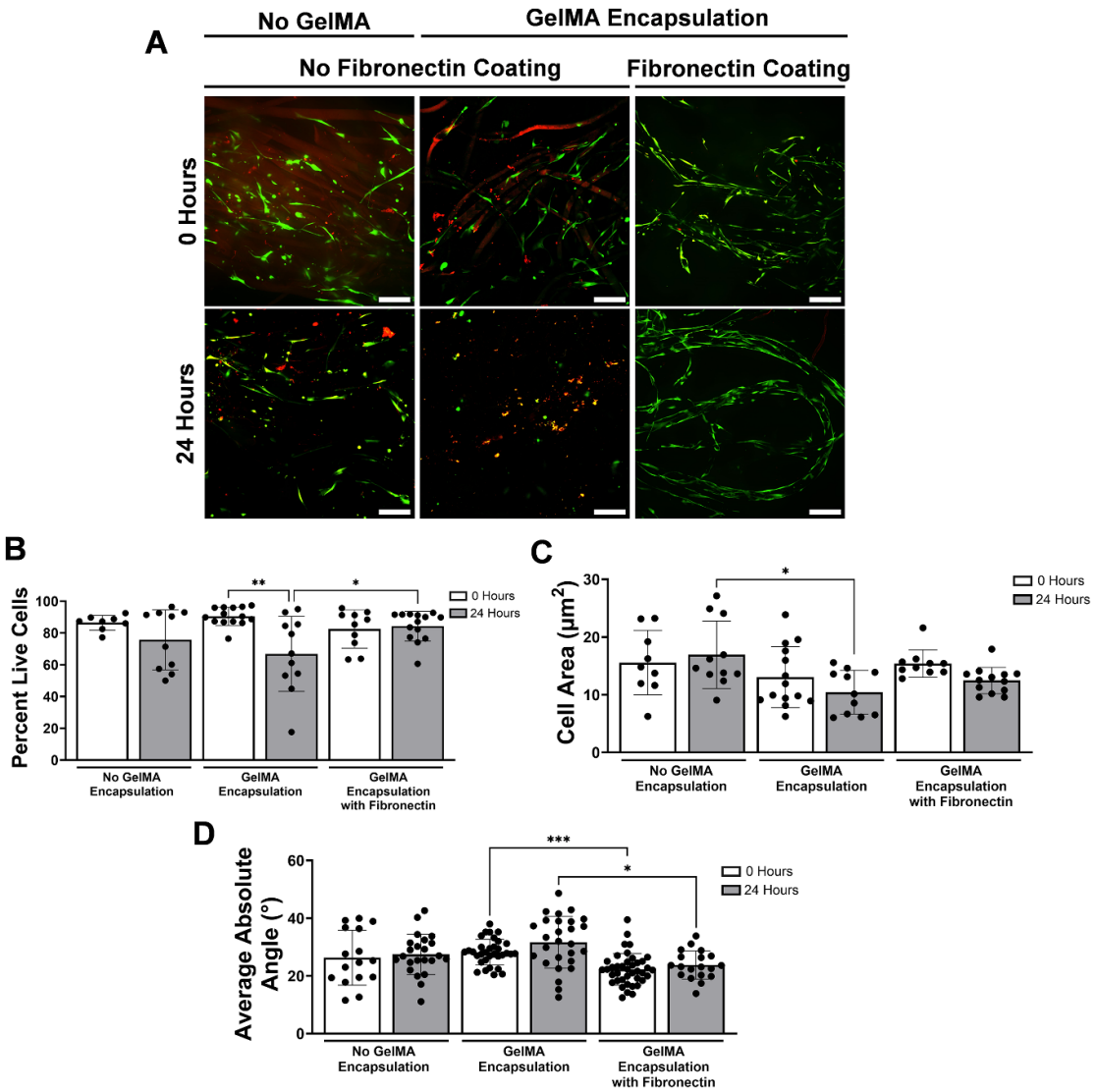

Figure 5. SMCs detached from microribbons when encapsulated in GelMA, but SMCs remained adhered to fibronectin-coated ribbons even after GelMA encapsulation. (A) Representative confocal microscopy images of SMCs on microribbons with and without GelMA encapsulation at 0 h and 24 h. Cells were labeled with calcein (green), indicating live cells and ethidium homodimer-1 (red), indicating dead cells. Scale bar = 200 μm. Quantification of the (B) percentage of live cells (n = 8–14 samples), (C) cell area (n = 8–14 samples), and (D) absolute angle (n = 16–40 individual microribbons from 8–14 samples). Statistical significance for (B)–(D) determined using a Kruskal–Wallis test. * $p < 0.05$, ** $p < 0.01$, *** $p < 0.001$.

area after GelMA encapsulation (figure 5(C)). Since fibronectin-coated microribbons enhanced cell adhesion after GelMA encapsulation, we used fibronectin-coated microribbons for the microribbon-lined channel.

Finally, we created the microribbon-lined channel by wrapping fibronectin-coated microribbons around a needle, encapsulating the microribbon-wrapped needle in GelMA, and then removing the needle. SMCs were then seeded on the inside surface of the channel. After 24 h in culture, SMCs inside the microribbon-lined channel maintained high viability (81% live cells), which was similar (p = 0.2101) to SMCs inside a channel without microribbons (86%; figures 6(A) and (B)). SMCs inside the microribbon-lined channel had a similar cell area (12 μm^2, p = 0.077) compared to SMCs inside a channel without microribbons (15 μm^2; figure 6(C). However, SMCs inside the microribbon-lined channel had higher cell alignment (p = 0.034), as shown by a lower average absolute angle (33°) as compared to SMCs inside a channel without microribbons (40°; figures 6(D) and (E)). Interestingly, SMCs in the channel without microribbons aligned axially along the channel while SMCs seeded on microribbons circumferentially aligned around the channel. With the single layer of SMC-coated microribbons, we achieved about 15% channel surface area coverage

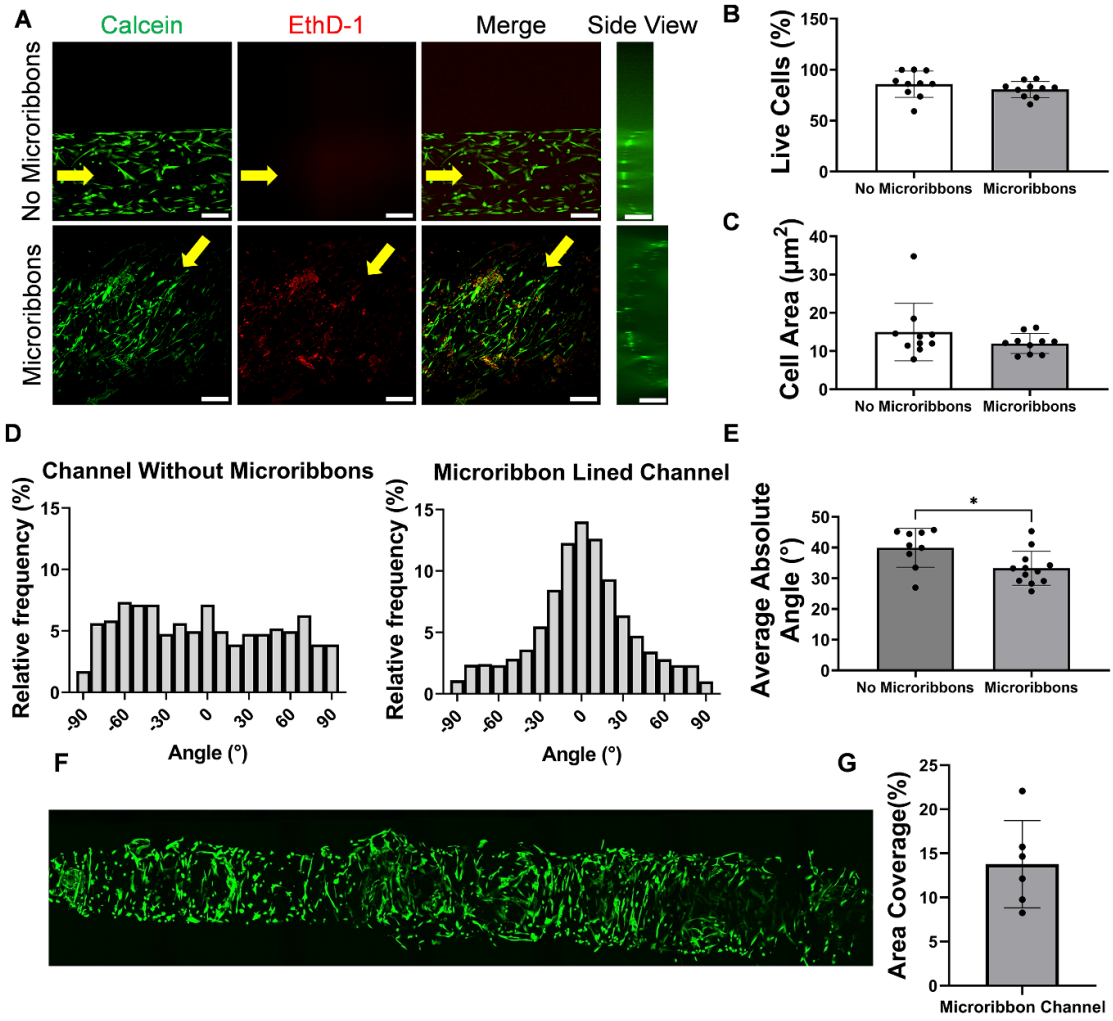

Figure 6. SMCs aligned circumferentially along wrapped microribbons in the GelMA channel. (A) Representative confocal microscopy images of calcein and ethidium homodimer-1 labeled SMCs seeded on the inside surface of channels with and without microribbons. The yellow arrow indicates the wrapped microribbon direction and the direction of the alignment quantification. Scale bar = 200 μm. Quantification of (B) percentage of live cells ($n = 10$ samples) and (C) average cell area ($n = 10$ samples). (D) Corresponding and representative cell alignment inside channels with and without microribbons, along with (E) average absolute angle ($n = 10$–12 individual microribbons from 10 samples). (F) Representative image with (G) quantification of calcein-labeled SMC area coverage along the microribbon lined channel. Statistical significance for (B), (C), (E) determined using a Mann–Whitney test. * $p < 0.05$.

(figures 6(F) and (G)). Together, these data show that SMCs can be circumferentially aligned inside a channel using circumferentially aligned gelatin microribbons.

4. Discussion

The gold standard to measure arterial health is vascular contractility, which is enabled by vSMCs [38]. As vSMC-induced vasocontraction and vasorelaxation in a native blood vessel requires their circumferential alignment around the blood vessel, it is essential to recapitulate this alignment in *in vitro* blood vessel models. In this study, we used gelatin microribbons with tunable thickness and stiffness to circumferentially align SMCs inside a cylindrical channel. This process enabled us to recapitulate native SMC alignment in a model blood vessel that is encapsulated in a hydrogel. In the future, the hydrogel could contain a parenchymal tissue (e.g. perivascular adipose tissue) that affects blood vessel function, and the vessel could be cannulated onto a pressure myography system to measure vasodilation and vasoconstriction. Therefore, our method could enable us to study vascular contraction and dilation using pressure myography in a physiologically relevant human *in vitro* model. This method could also be applied to other systems in which cells need to be aligned in a 3D hydrogel for *in vitro* studies (e.g. neurons and skeletal muscle cells).

To recapitulate *in vivo* vascular architecture and contractile function *in vitro*, it is essential to circumferentially align SMC around the blood vessel [18, 39]. When SMCs are aligned, they elongate into a spindle shape and produce more α-smooth muscle actin (α-SMA), which are key characteristics of the contractile phenotype observed in a healthy blood vessel *in vivo* [40]. Our method of

first circumferentially aligning gelatin microribbons inside a hydrogel channel served as a topographical cue that SMCs were able to follow. The technique is easy to implement and does not require complex methods or equipment to align the microribbons, as compared to other alignment techniques [24, 41]. Additionally, the described method is facile and low-cost as compared to commonly used patterning techniques such as electrospinning and soft lithography. Our method also enables investigators to form multiple layers of aligned SMC, similar to those in the vascular wall. For example, microribbons could first be wrapped around a larger diameter needle, seeded with SMCs, and inserted into the channel. Once that needle was removed, a smaller diameter needle wrapped with SMC-laden microribbons could then be inserted to create a second SMC layer. This process could be repeated, creating a series of concentric microribbon-lined channels using needles of different diameters. Alternatively, two SMC layers could be created by seeding SMCs on the inner surface of the hydrogel channel, followed by insertion of the needle wrapped with SMC-laden microribbons. In this procedure, a hydrogel that does not require UV crosslinking (e.g. collagen crosslinked with transglutaminase) would be preferred, as this would avoid UV crosslinking-associated toxicity for cells seeded on the hydrogel channel inner surface. Thus, our method is accessible and powerful in recreating multiple circumferentially aligned SMC layers [23, 41].

The gelatin microribbons designed in this study can easily be tuned to different thicknesses depending on their intended application. However, since the ribbons in our study were stretched and folded by hand, variability in the microribbons' thickness arose from non-uniform hand-stretching and narrowing of the ribbons. Notably, we found that as the number of folds exceeded 20 and the microribbons thinned to less than 1 μm, the uniformity of thickness significantly improved, though the underlying reason for this improvement remains unclear and warrants further investigation. To enhance thickness consistency, manual operation could be replaced by using an automated stretching and folding system, as suggested in our prior publication [29]. Compared to conventional methods that generate ribbon scaffolds, such as extrusion or wet spinning, the stretch-and-fold method generates gelatin microribbons on the cell size scale, allowing for easy control of cell alignment and shape [42–44]. When microribbons or ribbon scaffolds are too thin or thick, cells do not elongate along the fibers [29].

Similarly, the gelatin microribbons can be tuned to different stiffnesses. We decreased the MAA and increased the acetic anhydride to yield softer microribbons. This enabled us to create gelatin microribbons with a stiffness similar to that of the healthy vascular wall (~10 kPa) [37, 45]. Other ribbon scaffolds used to align cells are made of dextran or polycaprolactone, which have elastic moduli closer to 140 MPa and 3.8 GPa, respectively [46, 47]. Natural materials, such as silk and collagen fibers, still exhibit moduli close to 1.8 MPa and 1.5 GPa, respectively, which are orders of magnitude stiffer than the blood vessel wall [48, 49]. While these materials and techniques work well to recapitulate bone or cartilage biomechanics, they are not soft enough to replicate the native SMC niche in the blood vessel wall [50, 51]. Low substrate stiffness is critical to preserving SMC function and phenotype. Higher substrate stiffness increased SMC migration, proliferation, growth factor signaling, and cholesterol efflux [52–54]. For SMCs on aligned fibers, increasing stiffness from 15 MPa to 2142 MPa increased proliferation and lowered contractile marker expression [27]. Since our microribbon stiffness is tunable, we could create stiffer microribbons to mimic the stiffened vascular wall in aging or on the fibrous cap of atherosclerotic plaques, where the vessel stiffness increases to 30–90 kPa [55, 56].

Finally, the gelatin microribbons enabled us to independently tune both thickness and stiffness to best control cell alignment and function on the microribbons. Previous studies showed that intracellular localization of yes-associated protein (YAP) and transcriptional coactivator with PDX-binding motif (TAZ) depended on microribbon stiffness, alignment, and thickness [29]. When mechanotransduction signaling pathways are active, YAP/TAZ is translocated to the nucleus. In MSCs, it was found that when they were cultured on aligned microribbons that were soft (0.5 kPa) and thick (20 μm), YAP/TAZ was sequestered to the nucleus. For SMCs, YAP/TAZ localization to the nucleus suppresses vascular calcification and osteogenic differentiation, which enables a more contractile phenotype [57, 58]. In future studies, gelatin microribbon stiffness and thickness could be tuned to maximize SMC contractility.

While we employed gelatin microribbons to circumferentially align SMCs within a channel, our study is not without limitations. The human SMCs used in our studies adopt a proliferative phenotype *in vitro*. To test contractility in the future artery-on-a-chip, contractile SMCs should be used. The gelatin microribbons partially recreate the structure of the vascular wall extracellular matrix; however, the homogeneity of the microribbon material and its relatively simple structure cannot fully recreate the elastin lamellae, interlamellar fibers, and radial struts or the collagen fibers interspersed among the elastin lamellae [59]. A more representative model would include additional aspects of extracellular matrix architecture and binding sites, as well as multiple medial lamellar SMC units to generate multi-layer

vascular tissues. The channel developed using our technique can only be scaled down to the size of the needle around which the microribbons were wrapped. In this study, we used a 25 G needle, which is around 500 μm in diameter. To model arterioles or other types of vasculature, a smaller needle with an outer diameter of less than 100 μm would have to be used [60]. Furthermore, this technique requires manually wrapping the microribbons around the needle. As a result, there can be some variability in the microribbon layer thickness in the final channel. In future studies, automation of the microribbon wrapping process could enable formation of individual aligned microribbon layers with reduced biofabrication variability, which would better create thin circumferentially aligned SMC layers similar to a native blood vessel [61].

5. Conclusion

In this study, we used circumferentially aligned gelatin microribbons of tunable thicknesses and stiffnesses to circumferentially align SMCs inside a channel lumen. In the future, this technique will enable the creation of more physiologically relevant human *in vitro* models of vascular contractility.

Data availability statement

All data that support the findings of this study are included within the article (and any supplementary files).

Acknowledgments

This work was supported by the National Institutes of Health R21EB028466 and the National Science Foundation CBET-1916997 and CMMI-1751898.

Ethical statement

This study was performed in accordance with the Declaration of Helsinki. Human primary cell lines included in this study were approved as part of this study protocol. This human study was approved by the Institutional Biosafety Committee.

Author contributions

YM, L–HH, and AMC conceived and designed the research. YM, MK, MS, FA, and MF carried out the experiments. YM and MK analyzed data. YM, MK, LH, L–HH, and AMC interpreted results of experiments. YM, MK, and AMC prepared figures and drafted manuscript. YM, MK, MS, FA, PM, LH, L-HH, and AMC edited, revised, and approved the final version of the manuscript.

ORCID iDs

Yusuf Mastoor https://orcid.org/0000-0003-2760-9038
Mahsa Karimi https://orcid.org/0000-0002-9833-9699
Michael Sun https://orcid.org/0000-0002-6998-3266
Fereshteh Ahadi https://orcid.org/0009-0003-6757-0331
Mingyue Fan https://orcid.org/0000-0002-8365-7571
Lin Han https://orcid.org/0000-0003-4180-1288
Li-Hsin Han https://orcid.org/0000-0002-0135-2863
Alisa Morss Clyne https://orcid.org/0000-0003-2462-2122

References

[1] Virani S S *et al* 2021 Heart disease and stroke statistics-2021 update a report from the american heart association *Circulation* **143** e254–e743
[2] Libby P, Buring J E, Badimon L, Hansson G K, Deanfield J, Bittencourt M S, Tokgözoğlu L and Lewis E F 2019 Atherosclerosis *Nat. Rev. Dis. Primers* **5** 18
[3] Cyr A R, Huckaby L V, Shiva S S and Zuckerbraun B S 2020 Nitric oxide and endothelial dysfunction *Crit. Care Clin.* **36** 307–21
[4] Clyne A M 2021 Endothelial response to glucose: dysfunction, metabolism, and transport *Biochem. Soc. Trans.* **49** 313–25
[5] Chen K J, Pittman R N and Popel A S 2008 Nitric oxide in the vasculature: where does it come from and where does it go? A quantitative perspective *Antioxid. Redox Signaling* **10** 1185–98
[6] Schjorring O L, Carlsson R and Simonsen U 2015 Pressure myography to study the function and structure of isolated small arteries *Methods Mol. Biol.* **1339** 277–95
[7] Duling B R, Gore R W, Dacey R G and Damon D N 1981 Methods for isolation, cannulation, and in vitro study of single microvessels *Am. J. Physiol.* **241** H108–116
[8] Halpern W, Osol G and Coy G S 1984 Mechanical behavior of pressurized in vitro prearteriolar vessels determined with a video system *Ann. Biomed. Eng.* **12** 463–79
[9] Lawton P F, Lee M D, Saunter C D, Girkin J M, McCarron J G and Wilson C 2019 VasoTracker, a low-cost and open source pressure myograph system for vascular physiology *Front. Physiol.* **10** 99
[10] Delannoy E, Tellier G, Cholet J, Leroy A M, Treizebré A and Soncin F 2022 Multi-layered human blood vessels-on-chip design using double viscous finger patterning *Biomedicines* **10** 797
[11] Partyka P P, Godsey G A, Galie J R, Kosciuk M C, Acharya N K, Nagele R G and Galie P A 2017 Mechanical stress regulates transport in a compliant 3D model of the blood-brain barrier *Biomaterials* **115** 30–39
[12] Niklason L E, Gao J, Abbott W M, Hirschi K K, Houser S, Marini R and Langer R 1999 Functional arteries grown in vitro *Science* **284** 489–93
[13] Li Y H, Huang G, Zhang X, Wang L, Du Y, Lu T J and Xu F 2014 Engineering cell alignment in vitro *Biotechnol. Adv.* **32** 347–65
[14] Steucke K E, Tracy P V, Hald E S, Hall J L and Alford P W 2015 Vascular smooth muscle cell functional contractility depends on extracellular mechanical properties *J. Biomech.* **48** 3044–51

[15] Sumpio B E and Banes A J 1988 Response of porcine aortic smooth muscle cells to cyclic tensional deformation in culture *J. Surg. Res.* **44** 696–701
[16] Kim DH, Lipke E A, Kim P, Cheong R, Thompson S, Delannoy M, Suh KY, Tung L and Levchenko A 2010 Nanoscale cues regulate the structure and function of macroscopic cardiac tissue constructs *Proc. Natl Acad. Sci. USA* **107** 565–70
[17] Alford P W, Nesmith A P, Seywerd J N, Grosberg A and Parker K K 2011 Vascular smooth muscle contractility depends on cell shape *Integr. Biol.* **3** 1063–70
[18] Thakar R G, Cheng Q, Patel S, Chu J, Nasir M, Liepmann D, Komvopoulos K and Li S 2009 Cell-shape regulation of smooth muscle cell proliferation *Biophys. J.* **96** 3423–32
[19] Chang S, Song S, Lee J, Yoon J, Park J, Choi S, Park J K, Choi K and Choi C 2014 Phenotypic modulation of primary vascular smooth muscle cells by short-term culture on micropatterned substrate *PLoS One* **9** e88089
[20] Vo J, Mastoor Y, Mathieu P S and Clyne A M 2021 A simple method to align cells on 3D hydrogels using 3D printed molds *Adv. Biomed. Eng.* **1** 100001
[21] Hsiao A Y, Okitsu T, Onoe H, Kiyosawa M, Teramae H, Iwanaga S, Kazama T, Matsumoto T and Takeuchi S 2015 Smooth muscle-like tissue constructs with circumferentially oriented cells formed by the cell fiber technology *PLoS One* **10** e0119010
[22] Thakar R G, Ho F, Huang N F, Liepmann D and Li S 2003 Regulation of vascular smooth muscle cells by micropatterning *Biochem. Biophys. Res. Commun.* **307** 883–90
[23] Choi J S, Piao Y and Seo T S 2014 Circumferential alignment of vascular smooth muscle cells in a circular microfluidic channel *Biomaterials* **35** 63–70
[24] Sun T, Shi Q, Liang Q, Yao Y, Wang H, Sun J, Huang Q and Fukuda T 2020 Fabrication of vascular smooth muscle-like tissues based on self-organization of circumferentially aligned cells in microengineered hydrogels. *Lab Chip* **20** 3120–31
[25] Wang W Y, Davidson C D, Lin D and Brendon M B 2019 Actomyosin contractility-dependent matrix stretch and recoil induces rapid cell migration *Nat. Commun.* **10** 1186
[26] Baker B M and Mauck R L 2007 The effect of nanofiber alignment on the maturation of engineered meniscus constructs *Biomaterials* **28** 1967–77
[27] Yi B C, Shen Y, Tang H, Wang X, Li B and Zhang Y 2019 Stiffness of aligned fibers regulates the phenotypic expression of vascular smooth muscle cells *ACS Appl. Mater. Interfaces* **11** 6867–80
[28] Conrad B, Hayashi C and Yang F 2021 Gelatin-based microribbon hydrogels guided mesenchymal stem cells to undergo endochondral ossification in vivo with bone-mimicking mechanical strength *Regen. Eng. Transl. Med.* **7** 301–11
[29] Wang M, Cui C, Ibrahim M M, Han B, Li Q, Pacifici M, Lawrence J T R, Han L and Han L H 2019 Regulating mechanotransduction in three dimensions using sub-cellular scale, crosslinkable fibers of controlled diameter, stiffness, and alignment *Adv. Funct. Mater.* **29** 1808967
[30] Lee S, Tong X, Han LH, Behn A and Yang F 2016 Winner of the young investigator award of the society for biomaterials (USA) for 2016, 10th world biomaterials congress, May 17-22, 2016, Montreal QC, Canada: aligned microribbon-like hydrogels for guiding three-dimensional smooth muscle tissue regeneration *J. Biomed. Mater. Res.* A **104** 1064–71
[31] Conrad B, Han L H and Yang F 2018 Gelatin-based microribbon hydrogels accelerate cartilage formation by mesenchymal stem cells in three dimensions *Tissue Eng.* A **24** 1631–40
[32] Conrad B, Hayashi C and Yang F 2020 Gelatin-based microribbon hydrogels support robust msc osteogenesis across a broad range of stiffness *ACS Biomater. Sci. Eng.* **6** 3454–63
[33] Li Q, Qu F, Han B, Wang C, Li H, Mauck R L and Han L 2017 Micromechanical anisotropy and heterogeneity of the meniscus extracellular matrix *Acta Biomater.* **54** 356–66
[34] Dimitriadis E K, Horkay F, Maresca J, Kachar B and Chadwick R S 2002 Determination of elastic moduli of thin layers of soft material using the atomic force microscope *Biophys. J.* **82** 2798–810
[35] Ahearne M, Yang Y, El Haj A J, Then K Y and Liu KK 2005 Characterizing the viscoelastic properties of thin hydrogel-based constructs for tissue engineering applications *J. R. Soc. Interface* **2** 455–63
[36] Fomovsky G M and Holmes J W 2010 Evolution of scar structure, mechanics, and ventricular function after myocardial infarction in the rat *Am. J. Physiol. Heart. Circ. Physiol.* **298** H221–H228
[37] Savvopoulos F, Keeling M C, Carassiti D, Fogell N A, Patel M B, Naser J, Gavara N, de Silva R and Krams R 2024 Assessment of the nano-mechanical properties of healthy and atherosclerotic coronary arteries by atomic force microscopy *J. R. Soc. Interface* **21** 20230674
[38] Wenceslau C F *et al* 2021 Guidelines for the measurement of vascular function and structure in isolated arteries and veins *Am. J. Physiol. Heart. Circ. Physiol.* **321** H77–H111
[39] Richard M N, Deniset J F, Kneesh A L, Blackwood D and Pierce G N 2007 Mechanical stretching stimulates smooth muscle cell growth, nuclear protein import, and nuclear pore expression through mitogen-activated protein kinase activation *J. Biol. Chem.* **282** 23081–8
[40] Shen J Y, Chan-Park M B, He B, Zhu A P, Zhu X, Beuerman R W, Yang E B, Chen W and Chan V 2006 Three-dimensional microchannels in biodegradable polymeric films for control orientation and phenotype of vascular smooth muscle cells *Tissue Eng.* **12** 2229–40
[41] Agrawal A, Lee B H, Irvine S A, An J, Bhuthalingam R, Singh V, Low K Y, Chua C K and Venkatraman S S 2015 Smooth muscle cell alignment and phenotype control by melt spun polycaprolactone fibers for seeding of tissue engineered blood vessels *Int. J. Biomater.* **2015** 434876
[42] Street R M, Huseynova T, Xu X, Chandrasekaran P, Han L, Shih W Y, Shih WH and Schauer C L 2018 Variable piezoelectricity of electrospun chitin *Carbohydr. Polym.* **195** 218–24
[43] Qu F, Holloway J L, Esterhai J L, Burdick J A and Mauck R L 2017 Programmed biomolecule delivery to enable and direct cell migration for connective tissue repair *Nat. Commun.* **8** 1780
[44] Nathan A S, Baker B M, Nerurkar N L and Mauck R L 2011 Mechano-topographic modulation of stem cell nuclear shape on nanofibrous scaffolds *Acta Biomater.* **7** 57–66
[45] Laurent S, Girerd X, Mourad J J, Lacolley P, Beck L, Boutouyrie P, Mignot J P and Safar M 1994 Elastic modulus of the radial artery wall material is not increased in patients with essential hypertension *Arterioscler Thromb* **14** 1223–31
[46] Baker B M, Trappmann B, Wang W Y, Sakar M S, Kim I L, Shenoy V B, Burdick J A and Chen C S 2015 Cell-mediated fibre recruitment drives extracellular matrix mechanosensing in engineered fibrillar microenvironments *Nat. Mater.* **14** 1262–8
[47] Croisier F, Duwez AS, Jérôme C, Léonard A F, van der Werf K O, Dijkstra P J and Bennink M L 2012 Mechanical testing of electrospun PCL fibers *Acta Biomater.* **8** 218–24
[48] Johansson U, Widhe M, Shalaly N D, Arregui I L, Nilebäck L, Tasiopoulos C P, Åstrand C, Berggren PO, Gasser C and Hedhammar M 2019 Assembly of functionalized silk together with cells to obtain proliferative 3D cultures integrated in a network of ECM-like microfibers *Sci. Rep.* **9** 6291
[49] Yang L, van der Werf K O, Koopman B F J M, Subramaniam V, Bennink M L, Dijkstra P J and Feijen J 2007 Micromechanical bending of single collagen fibrils using atomic force microscopy *J. Biomed. Mater. Res.* A **82** 160–8

[50] Caro C G et al 2011 The Mechanics of the Circulation 2 edn (Cambridge University Press)
[51] Colin-York H, Eggeling C and Fritzsche M 2017 Dissection of mechanical force in living cells by super-resolved traction force microscopy Nat. Protoc. 12 783–96
[52] Brown X Q, Bartolak-Suki E, Williams C, Walker M L, Weaver V M and Wong J Y 2010 Effect of substrate stiffness and PDGF on the behavior of vascular smooth muscle cells: implications for atherosclerosis J. Cell. Physiol. 225 115–22
[53] Rickel A P, Sanyour H J, Leyda N A and Hong Z 2020 Extracellular matrix proteins and substrate stiffness synergistically regulate vascular smooth muscle cell migration and cortical cytoskeleton organization ACS Appl. Bio Mater. 3 2360–9
[54] Mao X, Tan Y, Wang H, Li S and Zhou Y 2021 Substrate stiffness regulates cholesterol efflux in smooth muscle cells Front. Cell Dev. Biol. 9 648715
[55] Rezvani-Sharif A, Tafazzoli-Shadpour M and Avolio A 2019 Progressive changes of elastic moduli of arterial wall and atherosclerotic plaque components during plaque development in human coronary arteries Med. Biol. Eng. Comput. 57 731–40
[56] Huynh J, Nishimura N, Rana K, Peloquin J M, Califano J P, Montague C R, King M R, Schaffer C B and Reinhart-King C A 2011 Age-related intimal stiffening enhances endothelial permeability and leukocyte transmigration Sci. Transl. Med. 3 112ra122
[57] Dupont S et al 2011 Role of YAP/TAZ in mechanotransduction Nature 474 179–83
[58] Wang L, Chennupati R, Jin YJ, Li R, Wang S, Günther S and Offermanns S 2020 YAP/TAZ are required to suppress osteogenic differentiation of vascular smooth muscle cells iScience 23 101860
[59] O'Connell M K, Murthy S, Phan S, XU C, Buchanan J, Spilker R, Dalman R, Zarins C, Denk W and Taylor C 2008 The three-dimensional micro- and nanostructure of the aortic medial lamellar unit measured using 3D confocal and electron microscopy imaging Matrix Biol. 27 171–81
[60] Rahman M and Siddik A B 2024 Anatomy, Arterioles, in StatPearls (Treasure Island (FL))
[61] Othman R, E Morris G, Shah D A, Hall S, Hall G, Wells K, Shakesheff K M and Dixon J E 2015 An automated fabrication strategy to create patterned tubular architectures at cell and tissue scales Biofabrication 7 025003